ORIGINAL ARTICLE

Biogeochemical plumbing of pioneer mangrove intertidal flats in French Guiana

Robert Aller[1] · Issac Klingensmith[1] · Thomas Stieglitz[2,3] · Christina Heilbrun[1] · Stuart Waugh[1] · Adelaide Aschenbroich[4] · Gerard Thouzeau[4] · Emma Michaud[4]

Abstract

Migrating mudbanks are characteristic features of the vast Amazon-Guianas coastline along Northeastern South America. As illustrated by sites in French Guiana, consolidating mudflats that periodically transition to mangrove forest are permeated by extensive crustacean burrow systems, sometimes in isolation but more often in close association with morpho-sedimentary structures such as tidal pools and channels. Burrow structures are critical to mangrove growth. In this study, we evaluated the ways in which burrows act as complex conduits that plumb deposits for solute exchange with overlying water. We sampled burrows during low tide when irrigation is inhibited and burrow water rapidly becomes anoxic. The products of diagenetic reactions, for example: NH_4^+, N_2, and $Si(OH)_4$, build up with time, revealing sedimentary reaction rates and fluxes. When oxygenated, burrow walls are zones of intense coupled redox reactions such as nitrification-denitrification. Build-up often is lower in burrows connected directly to tidal pools where photosynthetic activity consumes remineralized nutrients, and burrows can remain periodically irrigated at low tide. During flood, burrows, particularly those that connect tidal pools laterally to channels, can be rapidly flushed and oxygenated as channel water rises and then spreads across flats. Burrow flushing produces enhanced concentrations of nutrients within the leading edge of the flood as seawater moves progressively towards and into adjacent mangroves. Estimates of burrow volumes obtained from drone surveys together with burrow solute production rates allow upscaling of burrow-sourced metabolite fluxes; however, these are extremely variable due to variable burrow geometries, connections between burrows, pools, and channels, and burrow water residence times (oxygenation). The flushing of burrows during flood results in a rectification of sediment-water fluxes shoreward and enhances the delivery of nutrients from the flats into adjacent mangroves and pools, presumably stimulating colonization and forest growth.

Keywords Guiana coast mudbank processes · Crustacean burrow biogeochemistry · Burrow solute fluxes · Crustacean burrow-mangrove interactions

Communicated by Philippe Cuny and accepted by Topical Collection Chief Editor Christopher Reyer.

✉ Robert Aller
  robert.aller@stonybrook.edu

1   School of Marine and Atmospheric Sciences, Stony Brook University, Stony Brook, NY 11794-5000, USA

2   Aix Marseille Univ, CNRS, IRD, INRAE, CEREGE, 13545 Aix-en-Provence, France

3   Centre for Tropical Water and Aquatic Ecosystem Research (TropWATER), James Cook University, Townsville, QLD 4811, Australia

4   Univ Brest, CNRS, IRD, Ifremer, LEMAR, F-29280 Plouzané, France

Introduction

Approximately 15–20% of the Amazon River sediment outfall moves northwestward along Amapá, Brazil, and the Guianas, generating a vast muddy coastline that extends ~1600 km to the Orinoco River (Wells and Coleman 1978; Eisma et al. 1991; Baltzer et al. 2004; Anthony et al. 2010). This massive stream of mud propagates as a series of 20–25 shore-attached mudbanks migrating individually at ~0.5–4 km year⁻¹, eventually melding with the Orinoco Delta or leaving a small residual prograding shoreline (Allison et al. 2000; Allison and Lee 2004; Anthony et al. 2014). Mud-banks typically range in size from ~10–60 km alongshore, extend ~30–40 km cross-shore, and ~5–10-m maximum thickness (Augustinus 1978; 2004; Rine and Ginsburg

1985; Froidefond et al. 1988). As mudbanks propagate, inshore portions of the advancing mud stabilize, consolidate, and are quickly colonized by pioneering mangroves (Proisy et al.2009; Gensac et al. 2015). These mangroves grow rapidly (> 1 m year^{-1}) into dense forest ecosystems 10s of meters high (Fromard et al.1998; Proisy et al. 2009). The trailing edges of mudbanks are continuously eroded, remobilizing mud and removing mangroves, and the mixed sedimentary debris is recycled and translated to the leading edge over characteristic timescales of ~30 years (Allison and Lee 2004; Anthony et al. 2010). A critical stage in the establishment of mangrove forest during these periodic successional sequences is the initial colonization of stabilized mudflats by macroinfauna, and the resulting modification of sediment properties (Aschenbroich et al. 2017; Michaud et al. 2022). Of the colonizing faunal groups, brachyuran crabs in particular play a major role in mediating physical and biogeochemical conditions (Kristensen 2008; Stieglitz et al. 2013; Aschenbroich et al. 2016; Egawa et al. 2021; Michaud et al. 2022; 2024) which may be conducive for mangrove survival, productivity, and growth in these systems (Alongi 1997; Smith et al. 2009).

In the present contribution, we document and evaluate the impacts of biogeochemical processes associated with crab burrows in stabilized mudflats that are undergoing mangrove colonization along French Guiana. These biogenic structures create complex conduits that can typically extend ~0.1–0.4 m and up to ~1 m vertically, and 0.1–4 m horizontally within mudflats, depending on crab species, age, and location relative to morphological sedimentary features such as pools, platforms, and drainage channels (Michaud, et al. 2024). Our underlying hypothesis is that these burrow structures are a major component of the tidal flat processes governing sediment-water fluxes of diagenetically remineralized solutes (e.g., ΣCO_2; NH_4^+, $Si(OH)_4$), and sedimentary redox reaction coupling, for example, nitrification-denitrification and sulfide oxidation associated with oxygenation of anoxic sediment with overlying water. We utilize the time-dependent composition of water contained in burrows during tidal exposure as indicators of reaction pathways and rates in the tidal flat deposits and as a basis for estimating the impacts of burrows on solute fluxes into overlying water and adjacent regions (e.g., Aller and Yingst 1978; Aller et al. 1983). These individual measurements are upscaled using spatial distribution patterns of burrows documented independently with drones (Brunier et al. 2020; Michaud et al. 2024). Although any given mudflat benthic community and pioneering mangrove associations are ephemeral from a local perspective, the steady periodic properties of mudbank formation and removal imply that the mechanistic interactions gleaned locally within a representative depositional mudflat facies, such as in French Guiana, are broadly applicable to understanding dynamics and processes along the general coastal system.

Study site

A stabilized mudbank area located near the mouth of the Sinnamary River estuary, French Guiana (5°28′39″N–53°0′2″W) was sampled during the dry season (21–27 October 2014 and 15 November–15 December 2015) (Fig. 1). These deposits have since been entirely eroded and redeposited downstream. Tides near Sinnamary are semidiurnal with neap–spring tidal ranges of ~1–2.5 m (Michaud et al. 2024). Sampling of burrow water was carried out during spring low tides (LT) (2014; 3–3.2-m high tides (HT); 2015; 2.9–3.15 high tides (HT)) when burrow opening exposure times reached ~7–8 h. Mud on the shoreface is graded from very soft, relatively featureless deposits into a more consolidated mudbank dissected by drainage channels (~0.5–2-m width), pools (1–3-m scales), and open platform areas (Brunier et al. 2020). Where standing water was absent, surface mud (~1 cm) often became desiccated and polygonally cracked within 2–3 h of exposure to sunlight (Gardel et al. 2009), with visible precipitation of carbonate ($CaCO_3$), gypsum ($CaSO_4 \cdot 2H_2O$), and halite (NaCl) at the exposed sediment-water interface. Pioneering mangroves (0.05–0.7-m high) were intermittently scattered in the lower elevation portions of the flat. Seedlings were often initially situated in mudcracks, becoming more continuous in density and grading with mud elevation into larger juvenile mangroves (≥ 1-m high) (see representative images in Brunier et al. 2020; Supplement 1).

Methods

Tidal flat sampling—2014

Large burrow apertures characterizing complex burrows were preferentially grouped around pools and tidal flat channels (Brunier et al. 2020; Michaud et al. 2024) (Fig. 1D; Supplement 1). They were inhabited by a variety of infauna including crabs, shrimp, and fish (Michaud et al. 2024). Some pools remained filled with seawater, some partially drained, and some completely drained during low tide. Isolated burrows characterized by smaller apertures and inhabited by the fiddler crab *Uca maracoani* (Michaud et al. 2024) were less aggregated near sources of water at low tide and were distributed throughout the flat. The exposed burrow apertures associated with pools were sometimes filled to the level of the mudflat surface with seawater, or they were sometimes partially drained. For example, the water surface within burrows could be 10–15 cm below the upper mudflat surface although an immediately adjacent pool was filled. When burrows or a pool was
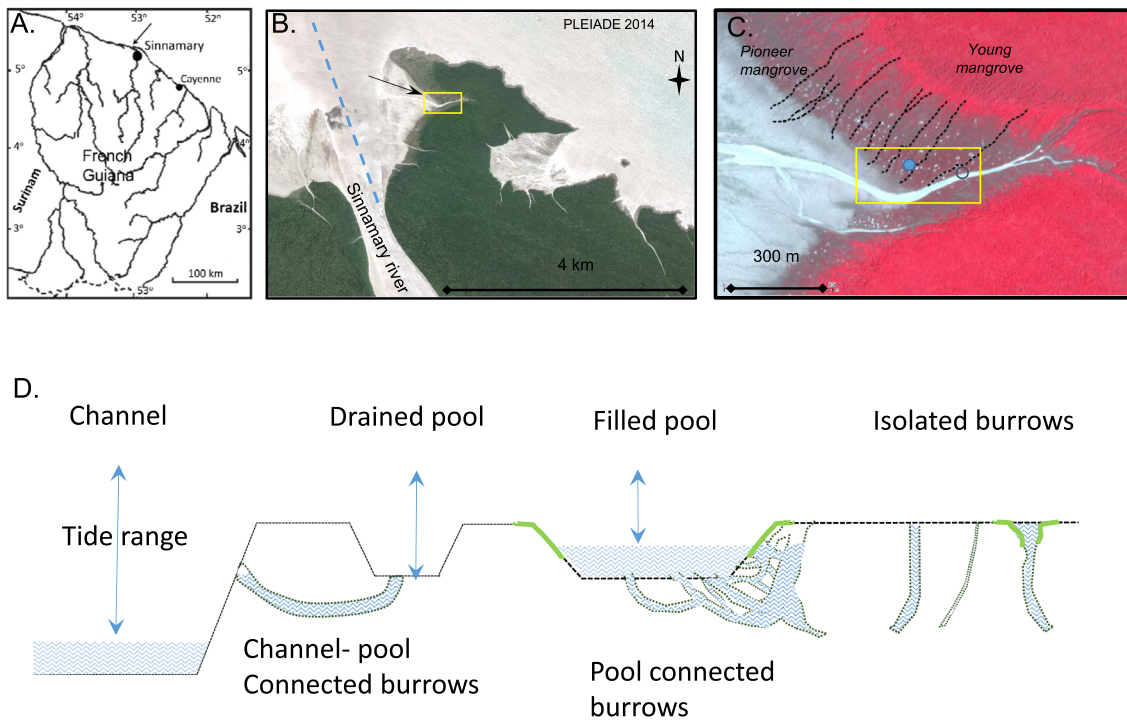
Fig. 1 **A** Map of French Guiana showing the location of the regional study area at the Sinnamary River mouth (arrow). **B** Satellite image of the Sinnamary River mouth region in 2014 with the location of both 2014 and 2015 sampling sites within a square (Astrium Services/PLEIADE images all rights reserved). The dashed line indicates an approximate transect line for overlying water samples (see also Ray et al. (2018)). **C** High-resolution image of study areas in 2014 (solid circle) and 2015 (open circle) (CNES - 2015; image processing in **B** and **A** by A. Ashenbroich, Université Bretagne Occidentale). **D** Schematic representation of biogenic burrow structures illustrating associations with morpho-sedimentary features within the sampled mudbank (green, microphytobenthos mats; blue stippled, water) (modified from Michaud et al. 2024)

selected for sampling, the time when they were isolated from receding overlying water was recorded, and time markers were placed around pools and any given burrow to be sampled. This permitted monitoring of time-dependent changes in the burrow and pool water composition following isolation from the larger overlying water reservoir. The overlying ebb water was sampled at the identified sampling location when 5–10-cm water depth remained. Overlying water was obtained in 1-L, wide-mouth polyethylene bottles and processed as described subsequently. The flood water was sampled in the same way (5–10-cm water depth) as the incoming water encroached and covered the flat. On one occasion (26 Oct. 2014), the water on the flat was also sampled successively at a single site during the flood when water was ~2-cm, 5-cm, and 10–15-cm depth. Temperature and light (LUX) conditions on the flat surface and within pools were monitored ($1 min^{-1}$) during daylight periods 22–27 Oct. 2014 using Onset HOBO temperature/light pendant microsensors tethered at the sediment surface.

During the 2014 campaign, time series burrow water sampling was focused within burrow aggregations around a tidal channel (22–25 Oct.) and around two pools that retained water throughout the entire ebb tide period (Oct. 25–26).

The level of water within the burrows remained the same as the adjacent connected pools or channel (Supplement 1). Several isolated burrows in the higher elevation platform of the flat were also sampled at a single time, although in each case, the exact time of their disconnection from overlying water was not measured. In one burrow that was connected horizontally to a tidal channel that crossed the flat from the main channel into the juvenile mangroves, oxygen and temperature sensors were inserted at the burrow entrance and bottom, and also at the entrance to the tidal channel. Sensors were monitored continuously (every 10 s) for 2 days (22–25 Oct., 2014). Separate measurements were made in the main channel overlying water. Continuous monitoring of burrow water and tidal channel oxygen and temperature was done with three optical IDS dissolved oxygen sensors (WTW FDO® 925). At a separate location, burrow and pool water were additionally sampled directly by inserting rhizon filters (5-cm long, 0.15-µm pore size; Rhizosphere Research Products) to a depth of ~10–15 cm in the case of burrows, or submerged below the water surface in the case of pool water, and extracting (without stirring) ~20 mL of water into an attached 60-mL polypropylene syringe. Care was taken not to have the rhizons contact the burrow walls and disturb

sediment, which was the primary factor limiting the depth of sampling. Burrow, pool, and overlying water were split into two ~8-mL subsamples (Wheaton polyethylene bottles). One sample was retained unacidified, and one was acidified to pH ~2 with trace metal grade HCl. A third sample for DIC and pH was retained in a 1- or 3-mL syringe without air space for later measurement in the lab. In the field, all water samples were rapidly placed into a cooler with icepacks. pH was measured in the lab with a semi-microelectrode (Thermo Scientific) referenced to NIST buffers at 28 °C.

Tidal flat sampling—2015

During the 2015 campaign, burrow water sampling was focused around one pool of many that remained full during low tide, scattered additional burrows within ~1 m of the primary pool (O_2, pH only—see subsequent methods), and a second pool that drained entirely but re-filled through burrows that were connected to a nearby major channel approximately 3–4 m away (Supplement 1). A subset of burrows near the filled pool was not actively connected to the pool (burrow water level lowered) while others remained at the pool water level and were assumed to be connected to the pool. Burrow and pool water were sampled with rhizons as described for 2014 samples, and in some cases by directly inserting O_2 and pH electrodes into pool and burrow water. Unfiltered samples were also taken separately for N_2 analyses. N_2 samples were withdrawn from burrows, pool water, and overlying channel water by syringe without bubble formation and immediately transferred to glass 12-mL Labco Exetainers (Lampeter, Wales, UK; labco.co.uk) for later dissolved gas analysis. Approximately 15 mL of sample was used to fill Exetainers to overflowing. Twenty microliters of saturated $HgCl_2$ was injected to each sample before sealing an Exetainer. Sealed Exetainer gas samples were stored in a cooler.

Two sets of sensors were used for the in situ burrow water measurements in 2015. In one set, measurements of water O_2, temperature, and pH were obtained by inserting electrodes/thermistor probe into burrows and pool water and recording the time-series output with a notebook computer. In the case of burrows, sensors were inserted initially into the water within the funnel-shaped aperture near the mudflat surface (~0–5 cm) and then to a depth of ~10–15 cm. It was not possible to insert sensors more deeply without disturbing the burrow wall and producing measurement artifacts. O_2 was measured using a robust (3 mm) FireSting optode (calibrated to atmospheric O_2) and thermistor temperature sensor, and a single channel meter (Pyroscience) linked to the notebook computer. pH was measured with a semi-microelectrode (Thermo Scientific) referenced to NIST buffers. The second sensor set was used on 28 Nov 2015 to measure salinity, temperature, and pH approximately hourly

during the low tide (LT 12:20) in the overlying water of a burrow near a pool, within the pool (channel-connected), and at three times in the adjacent tidal channel (LT−3h; LT; LT+4h). These sensors were part of a multiparameter water quality meter (WTW Multi 3500i) and had precisions of ± 0.1 salinity, ± 0.1 °C temperature, and pH ± 0.01%, the latter referenced to NBS buffers.

Overlying water offshore sampling—2014 and 2015

Overlying water offshore of the mudbank site was sampled for nutrient distributions as a function of salinity to help constrain the boundary conditions dictating the initial compositions of water ventilating burrows and pools. A set of 10 stations along a single transect in the main channel from the Sinnamary River mouth to further offshore was sampled during a flood on 21 Oct. 2014 in order to obtain surface water of variable salinities 0–33.2 (transect from 5° 25.869N; 52° 59.365W to 5° 29.888N; 53° 00.880W). Time series samples of surface water during a 12-h period on 30 October 2014 (HT; HT+3h; LT; LT+3h; HT) were obtained at three locations termed RIV (5° 27.276 N; 53° 00.721 W), SITE (5° 28.406 N; 53° 00.445 W), and MAR (5° 30.013 N; 53° 00.921 W). These sites were located to access surface water with relatively low (RIV), intermediate (SITE), and high (MAR) average salinities and to deploy current meters during a tidal cycle (Ray et al. 2018; only water compositions are considered here). Additionally, time series oxygen concentrations were monitored using a YSI multi-probe located in the main channel adjacent to the tidal flat channel where burrow oxygen and temperature were continuously monitored.

An overlying surface water sampling transect (12 stations) was also carried out in the main Sinnamary channel during flood tide on 5 Dec 2015. In all cases, water was sampled using 1-L wide-mouth polyethylene bottles and stored on icepacks in a cooler until returned to the field lab and then filtered and split into subsamples (unacidified, acidified, dissolved inorganic carbon (DIC)—see subsequent).

Analytical methods

Filtered, unacidified samples stored in 1–3-mL syringes without gas space were analyzed for DIC a few hours after acquisition (FIA-conductivity; Hall and Aller 1992). O_2, pH, and temperature were measured using a range of optical and electrochemical probes described previously under *Sampling* for each year. Other analyses were completed on stored samples at Stony Brook University. Chloride was measured using a Radiometer CMT-10 titrator (Ag^+–AgCl). Alkalinity, NH_4^+, $NO_3^- + NO_2^-$, and $Si(OH)_4$ were determined spectrophotometrically on stored unacidified samples using modifications of methods for application with

96-well plate readers (alkalinity-formic acid-bromophenol blue, Sarazin et al. 1999; NH_4^+, indophenol blue, Solórzano 1969; $NO_3^- + NO_2^-$-V reduction-Griess reagent, Doane and Horwath 2003; $Si(OH)_4$ molybdate blue, Strickland and Parsons 1972). N_2/Ar ratios in water samples were measured using MIMS (Kana et al. 1994; Waugh and Aller 2021). N_2 concentrations were calculated by multiplying the measured N_2/Ar ratios by the equilibrium value of Ar (at a temperature of analysis) derived from Hamme and Emerson (2004).

Results

Burrow, pool, and overlying water—2014

The exposed mudflat surface temperatures (2014 campaign) varied from ~27 to 46 °C (accuracy ± 0.5°), with minimum temperatures at daybreak and in the receding overlying water, and maximum temperatures at the sediment surface reached during midday. Filled pools had somewhat lower maximum temperatures of ~34–37 °C (Supplement 2). In 2014, temperature measured at the burrow water surface (5–15-cm depth) connected to the channel during the ebbing tide reached 35–38 °C at 1400 and decreased to 28 °C during the night until the sunrise (0600), while it was stable around 28–30 °C at the deeper sections of the burrow (30 cm) whatever the tides. Illumination, measured as lux (SI unit), at the sediment surface varied from 11 at daybreak to ~220,000 midday (single max 231,468) (sensor max 320,000; 10% reported accuracy). Lux in pool water (2–3-cm depth) was ~5000, sufficient to sustain microphytobenthic production.

O_2 concentrations in the overlying water of the channel and burrow top followed the same trends with similar values according to the ebbing and decreasing tides during the entire 24-h tidal cycle (shown later in Fig. 5A, B). They were the highest (~172 μM) at HT+1h and HT−1h with a decrease (~131 μM) at the peak of the high tide and the lowest at night during the low tide (16–22 μM). O_2 concentrations measured in the deeper parts of the burrow remained null (< 0.6 μM) during the 24-h tidal cycle (Fig. 5A, B).

The nutrient and alkalinity composition of burrow water changed progressively following disconnection from overlying water. NH_4^+, alkalinity, and $Si(OH)_4$ increased relatively regularly, reaching concentrations of ~130 μM, 2.95 mM, and 110 μM respectively (mM, millimolar; μM, micromolar; Figs. 2 and 3; Supplement 3). In contrast, NH_4^+, alkalinity, and $Si(OH)_4$ in adjacent pool waters were largely invariant over the same time period. Burrow waters were generally substantially elevated in these solute concentrations relative to the overlying water. Based on salinities in burrow water and overlying water variation with salinity, initial concentrations of $Si(OH)_4$ during active ventilation were ~10–60 μM, with most likely initially ~15–30 μM (Fig. 3B). Overlying water NH_4^+ ranged between 5 and 20 μM, and alkalinities from ~2 to 2.3 mM for burrow water chloride/salinity ranges (data not shown). Isolated burrow waters also had substantially elevated NH_4^+ concentrations relative to overlying water, reaching at least ~180 μM (Supplement 3). The overall rates of NH_4^+ and $Si(OH)_4$ concentration increases in the time series burrow samples were ~8.1 and 3.5 μM h^{-1} respectively (Figs. 2 and 3). A rough C/N ratio in burrow waters, not corrected for NH_4^+ adsorption losses, was ~6.1 mol/mol (Fig. 2C).

The pH of burrow waters in the 2014 sample sets was lower than pool waters by 0.1–0.4, and both burrow and pool waters increased with time of tidal flat exposure (BW-II
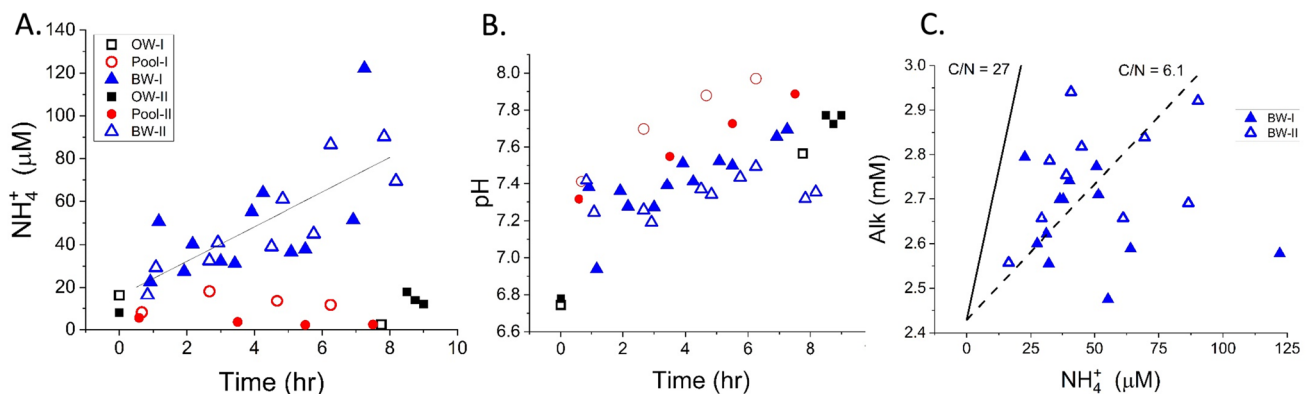

Fig. 2 **A** NH_4^+ as a function of time in ebbing and flooding water overlying mudbank platform site FG 2014 (OW-1; OW-2); pool water (Pool-1, Pool-2); and burrow waters (BW-I, BW-II). **B** pH (NIST) as a function of time (symbols as in **A**). **C** Alkalinity versus NH_4^+ concentrations in burrow waters (symbols as in **A**). Geometric mean regression (type 2) shown with C/N ratio 6.1 mol/mol (dashed line; r^2 = 0.07; not statistically significant). The expected trend for C/N = 27 (e.g., N poor mangrove substrate; Ray et al. 2018) is shown for comparison. The C/N geometric mean slope for DIC vs NH_4^+ in a 2015 burrow water set is 6.8 mol/mol (r^2 = 0.98; statistically significant; Supplement 4)
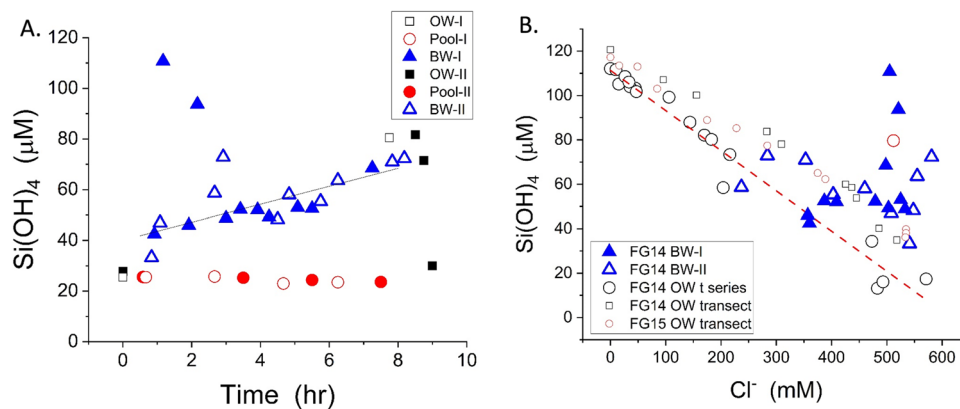
Fig. 3 **A** Si(OH)$_4$ as a function of time in ebbing (time 0) and flooding (~8–9 h) water overlying mudbank platform site FG 2014 (OW-1; OW-2); pool water (Pool-1, Pool-2); and burrow waters (BW-I, BW-II). Flood water (OW-II) shows a rapid drop in Si(OH)$_4$ as water depth increases from ~1 to 2 cm (leading edge) to 15 cm. **B** Compari-

son of Si(OH)$_4$ in overlying water within the Sinnamary River estuary channel (transect and time series) and burrow waters as a function of Cl$^-$ concentrations (salinity) in 2014. Si(OH)$_4$ versus Cl$^-$ in a surface water transect from November 2015 is also shown (FG15 OW)

slightly) (Fig. 2B). On 25 Oct., ebbing tidal flat water had a much lower pH, ~6.75, and elevated alkalinity, 3.0 mM, than incoming flood water which had pH ~7.8, alkalinity ~2.5 mM, at similar Cl$^-$ (512–513 mM). In comparison, on 26 Oct., ebbing tide flat water had a low pH of 6.77 and alkalinity of 2.73 mM at Cl$^-$ = 379 mM. The incoming flood water had a pH of ~7.7–7.8, alkalinities of 2.7–2.8 mM, and Cl$^-$ that progressively decreased from 589 to 554 mM as water depth increased from ~2 to 15 cm. The initial flood water was also elevated in Si(OH)$_4$, 81.7 μM, dropping rapidly to 29.9 μM as water depth increased (Fig. 3A).

Burrow, pool, and overlying water—2015

During the 2015 campaign, the sampled set of burrows associated with a single large pool showed highly variable behavior. The water height in several burrows dropped a

few centimeters despite a stable height in the adjacent pool, and then the burrow water heights stabilized. These burrows showed a progressive increase in NH$_4^+$, alkalinity, N$_2$, and Si(OH)$_4$, and a decrease in NO$_3^-$ (Figs. 4 and 5), reaching maximum concentrations of 189 μM, 2.31 mM, 422 μM, and 189 μM, and a minimum of 0 μM (NO$_3^-$) in 3–4 h. In contrast, the nutrient composition of the adjacent pool (T increase to 37 °C) was relatively constant. Those burrows that were apparently connected to the pool, based on stable and similar water heights, also showed solute compositions comparable to the pool (Fig. 4). Burrow water temperature measured using the thermistor probe (Pyroscience) at 5–15-cm depth varied from ~27.8 to 28.3 °C.

The initial rates of change of NH$_4^+$, NO$_3^-$, N$_2$, and Si(OH)$_4$ of water in burrows that apparently did not exchange directly with the pool water were ~52, −0.97, 14, and 48 μM h^{-1} respectively (0–3.6 h). In these cases,
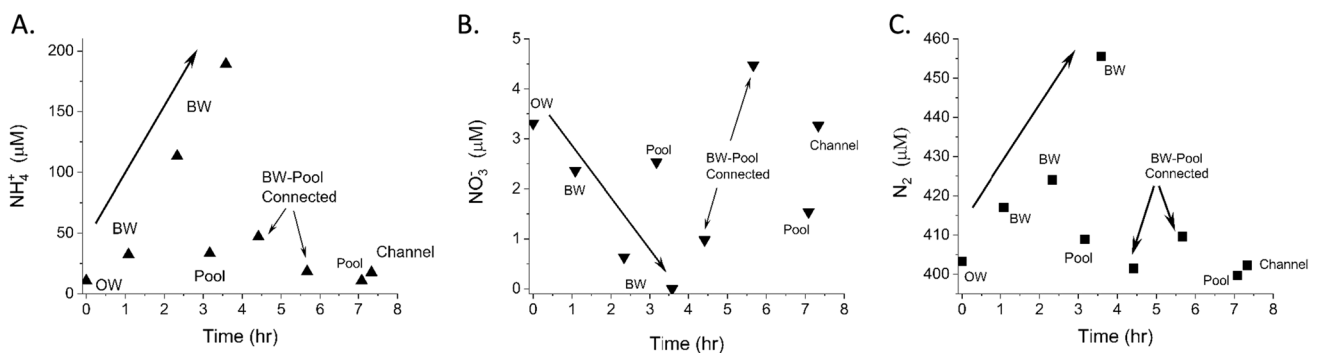

Fig. 4 Time series burrow waters, associated pool water, ebb overlying water, and channel flood water concentrations of NH$_4^+$, NO$_3^-$, and N$_2$ at a single pool site during 2015 sampling. Initial time series burrow water (to ~3.6 h) reflects separate individual burrows. If the

initial conditions were the same within all burrows, the trend corresponds to net fluxes. Burrows connected to the adjacent pool are indicated as BW-Pool connected
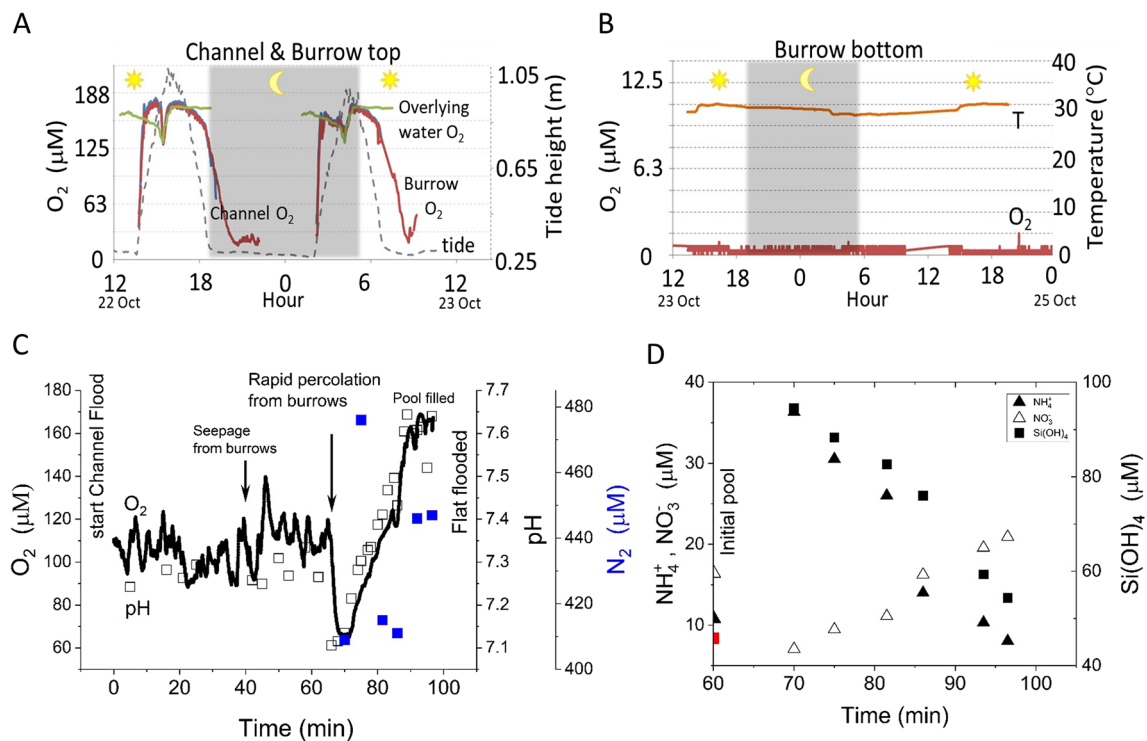
Fig. 5 A Time series O$_2$, tidal height (gray), in main Sinnamary channel (blue), tidal flat channel (green), and burrow top (red) over a 2-day period (2014) (no data periods, no water over the sensor at low tide). **B** Time series O$_2$ (red) and temperature (orange) at the bottom of the burrow demonstrating O$_2$ < 1 μM and temperature stability over a 2-day period. **C** Time series compositions of pool water (2015) connected through burrows with the adjacent tidal channel (3–4-m distance) during the flood. Time 0 represents the approximate time of the initial flood within the adjacent channel. Flood water topped the pool edge at ~97 min after initial tidal channel flooding. O$_2$, pH, and N$_2$ varied within the residual pool (~0.5 cm depth of water), during the progressive initial seepage evident from burrows, rapid flow (percolation) through burrows (~65–70 min) into the pool, and overbank flood of the pool (~97 min). **D** NH$_4$+, NO$_3^-$, and Si(OH)$_4$ compositions of pool water when burrow water is flushed into the pool as the channel water purges the connecting burrow conduits (time as in **C**). The composition of the water that initially filled the pool (and surrounding flat) before it drained at ebb tide is plotted for reference at 60 min (actual sampling time was −345 min relative to 0 time in **C**)

Cl$^-$ concentrations in the burrow and pool water averaged 425 ± 14 mM (salinity = 33.6) for samples up to ~7 h when pool and channel water were 359 and 373 mM (salinity = 23–23.9) respectively (Supplement 4).

In contrast to the burrows monitored in 2014, the pH of water in burrows sampled in 2015 decreased with time of isolation from overlying water or remained distinctly lower (6.5–6.8) than overlying water and pool water (Supplement 5, Supplement 6 – Figure). Burrow water pH varied inversely with NH$_4^+$ (Supplement 6 – Figure). During the same tidal period (28 Nov 2015), alkalinity was variable, generally 1.9–2.3 mM, while DIC reached 3.6 mM. One burrow water sample (at 3.6 h) had a very low pH = 6.68 and a low alkalinity of 1.04 mM (DIC = 2.41 mM). Ignoring the time point at 3.6 h, there was an overall geometric mean relation between DIC/Alk ~3.8 (r^2 = 0.57) in samples (Supplement 4 data). The Si/NH$_4^+$ correlation was 0.88 mol/mol (geometric mean; r^2 = 0.85), although these solutes are not necessarily coupled by common reactions during remineralization (i.e., correlation with time not reaction stoichiometry).

The O$_2$ concentrations within individual burrows (2015) were highly variable. When funnel-shaped apertures were filled with water and exposed to sunlight, microphytobenthos formed a distinct green surface layer within the funnel region, and O$_2$ became supersaturated in the upper ~5 cm of burrow water after tidal exposure. O$_2$ measured in the exposed aperture of eight burrows was 27–46% relative to equilibrium saturation of ~21% (1.3–2.2× saturation; T = 28–29 °C). O$_2$ in four burrows where water had dropped below the funnel region (shaded) to depths of 10–15 cm was 0–0.5% (0–0.02× saturation). The salinities of burrow waters in these cases were not measured, so the O$_2$ concentrations are approximate. Assuming that these burrow waters were comparable in salinity to pool water (32–34.8), then O$_2$ 100% saturation was likely ~200 μM (T = 28–29 °C).

One pool (2015) located ~3–4 m from a large tidal channel drained completely during low tide (Supplement 1). The residual water was ~0.5-cm depth within small puddles in

the pool and retained a relatively low O_2 (110 μM) and pH (7.24) despite direct exposure to the atmosphere (Fig. 5C). As the adjacent channel filled during flood tide, water began to seep from burrow openings in the bottom of the pool before the tide overtopped the side of the channel and covered the flat. Water continued to fill the pool and was eventually full at the same time the surrounding flat surface itself became flooded and tidal flat water merged with the pool. As it filled, the composition of the water in the pool changed continuously, reaching a minimum O_2 of ~65 μM and pH ~7.1 at ~70 min after the channel flood began when water clearly began percolating rapidly from burrow openings into the bottom of the pool (Fig. 5C). Water entering the pool through burrows became progressively higher in O_2, pH, and N_2, the latter reaching a supersaturated value in one sample of ~475 μM and in two others at ~446–447 μM. During the same period as the pool flooded, NH_4^+ decreased progressively from ~36 to 8 μM, NO_3^- increased from ~7 to 21 μM, and $Si(OH)_4$ decreased from ~95 to 54 μM (Fig. 5D), eventually obtaining concentrations that were present on the flat and pool during the previous ebbing tide and within the flooding channel (see FG15 OW transect $Si(OH)_4$, Fig. 3B). The $Si(OH)_4/NH_4^+$ ratio in the pool during flood was 1.37 mol/mol (geometric regression; $r^2 = 0.91$). DIC decreased from 2.11 to 1.94 mM during pool flooding, with a C/N stoichiometric relation of 6.8 mol/mol (geometric mean regression; $r^2 = 0.98$) (Supplement 4). The DIC/Alk geometric regression slope over the same pool flooding sample set was 0.74 mol/mol ($r^2 = 0.83$). Cl^- showed little variation in the same samples (average 505 ± 3 mM; salinity 32.3 ± 0.2).

The salinity, temperature, and pH were measured during the low tide (LT 12:20) in the overlying water of a burrow near a pool and of the pool (channel-connected), and at three time periods in the adjacent tidal channel (LT−3h; LT; LT+4h), demonstrated the isolation of the burrow from the pool in this case (Supplement 5). Salinities in the pool were ~33.3 ± 0.2, temperature increased progressively from ~29.9 to 37.6 °C, and pH increased slightly from 7.60 to 7.75 over ~6.5 h. In contrast, burrow water salinities dropped progressively from ~31 to ~24 (reason unknown); the temperature was approximately stable at ~30 ± 0.8 °C; and pH was approximately stable at 6.57 ± 0.1, although both temperature and pH show a tendency to increase slightly.

Discussion

Burrow water solute composition patterns

Burrow water solute compositions measured in both the 2014 and 2015 campaigns varied as a function of time and with the specific connections of burrows with pools and tidal channels. The sampled burrows were in the "large"

burrow opening category of Michaud et al. (2024), which do not dominate numerically with respect to surface opening abundances but dominate subsurface burrow volumes. Solute compositional changes apparently reflected combined remineralization and metabolite reoxidation reactions. Variable contributions of these reactions were associated with burrow walls and with ambient bulk sediment deposits in diffusive proximity to burrows. The different reaction balances evident in burrow water solute dynamics (e.g., DIC, alkalinity relations) during low tide demonstrate the highly complex coupling of burrows with overlying water over tidal timescales. We note that these deposits are very fine-grained, relatively consolidated, and have low permeability, minimizing the influence of pore water advective flows through other than the burrow lumens (see conductivity sensor data of Michaud et al. 2024).

We did not detect any deviations of burrow water from major element solute compositions of seawater relative to Cl^- (Mg^{2+}, Ca^{2+}, Na^+, K^+—measured using ICP–OES (inductively coupled plasma–optical emission spectroscopy); invariant composition data not otherwise reported). Because of the sampling design, all compositional patterns reflected unsteady changes associated with the initial isolation of burrows from ventilation with overlying water (Figs. 2, 3, 4, and 5; Supplement 3–6), connection with isolated bodies of water represented by pools (Figs. 4 and 5; Supplement 1), connection with tidal channels, or the flushing of burrows by overlying water during flood (Fig. 5; Supplement 1). The rates of change in solute concentrations reflect the diagenetic reaction balances within surrounding sediment, the exchange of solutes with burrow walls, the subsurface geometry and sizes of burrows, and the residence times of burrow water within different sectors of burrows. Compositions within individual burrows, for example, O_2, likely varied throughout different sectors and galleries of these complex geometric structures as shown by the difference of DO concentrations between burrow surface and bottom (e.g., Fig. 5; Forster 1991; Ziebis et al. 1996; Bertics et al. 2010) but likely also varied throughout the tidal cycle.

There are some consistent compositional patterns. In virtually all cases, although not necessarily coupled by common reactions, both NH_4^+ and $Si(OH)_4$ increased with time and were substantially elevated relative to measurements in overlying water at equivalent salinities (Figs. 2 and 3; Supplement 4). Burrow water NO_3^- was typically lower than overlying water, and N_2 was often elevated relative to atmospheric saturation, indicative of net denitrification and or anammox in at least parts of burrows and suboxic conditions (Figs. 4 and 5). There was no evidence of net N_2 fixation (N_2 depletion relative to atmospheric saturation), although simultaneous N_2 fixation and denitrification are possible (Bertics et al. 2010; Waugh and Aller 2017). The substantial mismatch in the

rates of NO_3^- decrease (-0.97 μM h^{-1}) and N_2 increase (14 μM h^{-1}) in burrow water (e.g., Fig. 4) demonstrates that most NO_3^- supporting denitrification and/or anammox must be produced by nitrification within the oxygenated zones of the burrow walls and is closely coupled to N_2 production. The enhancement of net N_2 production associated with burrows is consistent with many studies that have demonstrated stimulation of coupled nitrification-denitrification by bioturbation activities (e.g., Kristensen and Kostka 2005; Waugh and Aller 2017); however, Otero et al. (2020) inferred the opposite effect based on enhanced N_2O release from defaunated areas of mangroves in Northeastern Brazil.

Alkalinity and DIC relationships are also consistent with a contribution of denitrification to burrow water compositions, most specifically in the FG2015 sample series where ΔDIC/ΔAlk exceeded 1 (Δ indicates a change in DIC relative to change in alkalinity, i.e., the slope of regression) in one sample set (Fig. 4). However, the ΔDIC/ΔAlk ratio was substantially greater than ~1.05 (Redfield stoichiometry) implying that overall stoichiometric balances within burrow waters reflect multiple reactions such as metabolite reoxidation that contribute simultaneously to the net solute fluxes within burrows. For example, FeS_2 (pyrite) oxidation may titrate alkalinity and lower pH, a reaction that may account for the extreme excursion of pH and alkalinity in at least one sample of the FG2015 series. It is likely that such metabolite oxidation reactions take place continuously in different regions and times within burrows during oxygenation-deoxygenation cycling. These reoxidation reactions during bioturbation can lower the overall storage of anaerobic products such as Fe-sulfides (e.g., Araújo et al 2012).

In contrast to the elevated ΔDIC/ΔAlk (i.e., > 1) in the burrow set associated with the filled pool, the ratio was < 1 when burrows connected to the nearby tidal channel were progressively flushed during the flood to refill the pool that drained during low tide (Fig. 5). In this case, it is likely that combinations of Fe, Mn-oxide reduction in burrow walls and surrounding sediment, and/or carbonate mineral dissolution account for a ΔDIC/ΔAlk ratio of ~0.74 mol/mol during flushing despite concomitant denitrification as indicated by the supersaturated N_2 concentrations. Under conditions of multiple simultaneous anaerobic and aerobic remineralization, metabolite reoxidation, and photosynthetic (in burrow apertures) reactions, pH change patterns can also be complex (Soetaert et al. 2007), and we observed both increases and decreases of pH with time within burrow water (Figs. 3 and 5). These variable overall stoichiometric relations demonstrate that diagenetic reaction balances within the burrows can be highly complex with likely different net impacts on DIC—alkalinity relationships as a function of time, burrow association with morpho-sedimentary structures, and

sectors—galleries within individual burrows (e.g., Forster 1991; Ziebis et al. 1996).

Although there are substantial uncertainties (i.e., no statistical significance), the C/N stoichiometries implied by DIC, alkalinity, and NH_4^+ relationships suggest that the primary reactive organic substrate supporting solute production in the deposits is likely dominated by marine organic matter sources (C/N ~6.1–6.8) and not mangrove debris (C/N ~15–27; Ray et al. 2018). Such dominance would be consistent with both the C isotope composition of DIC and DOC ($\delta^{13}C$) and the C/N remineralization stoichiometries observed in offshore remobilized mud deposits that entrain marine plankton and become the consolidated mudbanks, and with the major contribution of microphytobenthos to reactive substrates incorporated into mudbank deposits and adjacent channel waters (Aller et al. 2004; Aller and Blair 2006; Gontharet et al. 2014; Ray et al. 2018).

The fact that burrow water in the funnel aperture openings of large burrows was often supersaturated with O_2 due to microphytobenthos photosynthetic activity demonstrates that the flared funnel morphology promotes O_2 in the near-surface zone of burrows during tidal exposure. These large aperture burrows often seemed not to be actively maintained by crabs (e.g., no excavated sediment, no sediment mixing around, neither grazing or pellets activities), but the structures favor microphytobenthos development (Michaud et al. 2024). Funnel morphologies can also act as sediment traps and a means of enhancing organic-rich particle delivery as a food resource (e.g., Iribarne et al. 2000). Thus, an increase of both reductant (organic matter) and oxidant (dissolved O_2 from microphytobenthos) supply to burrow occupants can apparently occur as a result of the funnel shape. Overall, the measurement of either low concentrations or the absence of dissolved O_2 in burrows below ~10–15-cm depth, and solute compositions such as supersaturated N_2 indicate that suboxic to anoxic burrow wall conditions are common, as found in other crustacean burrow structures (Ziebis et al. 1996). Although Fe^{2+} in burrow waters was not measured in this study, Fe-reduction generally dominates in these deposits (Aller et al. 2004; unpublished Fe^{2+} sensor data), and, together with denitrification-anammox, is a likely major component of suboxic diagenetic reactions in the burrow walls (e.g., Kristensen 2008; Kristensen et al. 2011).

Solute fluxes from burrows

As demonstrated by the data obtained in this study and previously, the solute compositions in burrows within the mudbank deposits are governed by a variety of factors related to burrow geometries (morphologies), species-specific burrow wall construction, burrow spacing, water ventilation patterns and residence times within burrow sectors, active or inactive habitation, associations with morpho-sedimentary

structures (pools, channels), unsteady burrow wall reaction patterns, and the reactivity of the bulk mudbank sediment within which burrows are formed. These factors result in variable contributions of remineralization reactions (e.g., aerobic, denitrification, Fe-reduction), metabolite reoxidation, and photosynthesis (microphytobenthos) to water compositions within individual burrows at different times and locations within the mudbank facies. The multiple factors involved mean that in contrast to the total flux of water through burrows, most diagenetically produced or consumed solute fluxes cannot, for example, simply be estimated from the flux of natural radionuclide tracers from burrows, the latter being governed by approximately fixed sources and known reaction rates within ambient bulk sediment (e.g., ^{226}Ra activities; ^{222}Rn production rates; Stieglitz et al. 2013). Likewise, general increases in fluid conductivity of mudbank facies by burrows cannot be readily translated into reactive solute fluxes or rates of aerobic metabolism (e.g., Xin et al. 2009; Guimond et al. 2020) without a statistical weighting of species and size-specific burrows, biogeochemical microenvironments, and ambient sediment remineralization rates (e.g., reactive organic matter inventories—mudbank age) relative to the total water flux (e.g., Agusto et al. 2021).

Although accurate estimates of benthic fluxes are not possible given the present limited data, likely general ranges of remineralized solute exchange contributed by subsurface biogenic structures can be calculated using the total burrow volumes inferred from drone reconnaissance and burrow aperture/subsurface volume relationships documented for the dominant *Uca* spp. and additional infauna by Michaud et al. (2024) and Brunier et al. (2020). The range of burrow volumes is highly variable: 0.03–20 L m^{-2}, depending on associations (or not) of burrow structures with morphosedimentary features. The spatial average (platform, pools, channel edges) over the study sites (2015) based on drone surveys integrating burrow patterns of the mudbank is ~0.35 L m^{-2}, with a median of 0.21 L m^{-2} (Michaud et al. 2024). If we assume that the initial rates of change of solute concentrations of solutes within burrows during low tide are indicative of reaction rates throughout a tidal cycle, the ranges of NH$_4^+$, N$_2$, and Si(OH)$_4$ production rates within burrows are 8.1–52 (NH$_4^+$), 14 (N$_2$), and 3.5–48 (Si(OH)$_4$ μM h^{-1}. These ranges, together with the spatially averaged burrow volume, translate into mudbank scale fluxes from burrows of 0.07–0.4 (NH$_4^+$), 0.1 (N$_2$), and 0.02–0.4 (Si(OH)$_4$) mmol m^{-2} day^{-1}. In areas where burrows are aggregated and contribute enhanced burrow volumes, for example, near pools: the drone-derived average volume increases to ~0.85 L m^{-2} (with directly measured local averages of ~10 L m^{-2}; maximum ~20 L m^{-2}; Michaud et al. 2024), increasing these average fluxes to ranges of 0.2–1 (NH$_4^+$), 0.2 (N$_2$), and 0.5–1 (Si(OH)$_4$) mmol m^{-2} day^{-1}. Enhancements of DIC-alkalinity fluxes from burrows must be similarly variable and related very roughly to N fluxes

by a C/N ratio of ~6 (Fig. 2D), suggesting that on average, they represent a relatively minor fraction of the estimated DIC exported from the mangrove system of ~75 mmol m^{-2} day^{-1} (Ray et al. 2020). When maximum burrow volumes are reached locally the fluxes could be ~10–20 × these ranges. Thus, the contribution of burrows to sediment-water fluxes is clearly highly variable spatially and can range from relatively small to extremely large contributions locally depending on burrow size and density patterns. In the case of redox-sensitive reactions such as nitrification-denitrification, and metal fluxes such as Fe^{2+} and Mn^{2+}, the variability of O$_2$ dynamics (e.g., Fig. 5) within burrows, coupled with burrow geometry variability, implies biogeochemical diversity, highly variable reaction balances, and reactive solute fluxes across the flats.

Regardless of the exact flux enhancement, one of the interesting interactions between burrows and tidal cycles is the rectification of sediment-water fluxes that occur because of solute build-up during low tide and flushing of burrows during the flood. The maximum concentrations of remineralized solutes and reaction products, and depletion of O$_2$, within burrows generally occur at the end of low tide (e.g., Figs. 2, 3, 4, and 5). As flood waters enriched in oxygen move onto the mudbank and flush burrows, the leading edge of the flood becomes differentially enriched in nutrients contributed by burrows and the dissolution of evaporite minerals that formed during desiccation at low tide (Figs. 2 and 3). This enriched water, a few centimeters in depth, moves towards the higher elevations of the mudbank colonized by juvenile mangroves. The focusing of regenerated nutrients in this manner may enhance microphytobenthos productivity and associated bioturbation activity in elevated zones of flats and directly and indirectly provide a positive feedback on juvenile mangrove growth.

Conclusions

Burrow water solute compositions in French Guiana mudbank deposits are generally characterized by enhanced concentrations of remineralized solutes (NH$_4^+$, Si(OH)$_4$, N$_2$) and reoxidized metabolites (pH, DIC-alkalinity relations) relative to overlying waters that largely reflect suboxic and anoxic diagenetic reactions in burrow walls and ambient sediment. Compositions are time-dependent, and net reaction stoichiometries can be complex due to variable contributions of multiple, simultaneous reactions, various degrees of exchange and water residence times depending on association with pools and channels, burrow geometries and densities, and the reactivity of organic substrates in burrow walls and ambient sediment. Oxygen concentrations are generally low in isolated burrow waters but can vary widely between supersaturation in funnel apertures near the sediment-water interface (0–5 cm) and below detection at depth in the same burrows (e.g.,

10–15 cm). The complexity and variability of nonconservative (reactive) solute compositions within burrow structures mean that total water flow and bulk conductivity changes of deposits induced by burrow structures may not relate in any simple way to sediment-water fluxes of reactive solutes. The variability of burrow water compositions and burrow abundances of different sizes and geometries prevents exact upscaled estimates of remineralized solute fluxes from burrows. Where burrows are aggregated, for example, around pools, it is clear that substantial contributions from burrows to the sediment-water fluxes of solutes such as NH_4^+, N_2, and $Si(OH)_4$ can occur (e.g., in the localized extreme of ~1–20 mmol m^{-2} day^{-1}). Thus, burrows are proximal sources of dissolved nutrients (Si, N) to overlying water but are also sites of net N loss (denitrification-anammox) to the ecosystem. The coupling of tidal flooding of the flat with flushing of burrows results in a rectification of regenerated nutrient fluxes from the lower towards the higher elevation regions of the mudbank, presumably promoting microphytobenthic primary production, associated bioturbation activity, and mangrove colonization and growth. These findings demonstrate the highly complex interactions of infaunal burrows and morpho-sedimentary structure with biogeochemical cycling and ecosystem functions of coastal mudbanks and mangrove forests.

References

Agusto LE, Fratini S, Jimenez PJ, Quadros A, Cannicci S (2021) Structural characteristics of crab burrows in Hong Kong mangrove forests and their role in ecosystem engineering. Estuar Coast Shelf Sci 248:106973. https://doi.org/10.1016/j.ecss.2020.106973

Aller RC, Blair NE (2006) Carbon remineralization in the Amazon-Guianas tropical mobile mudbelt: a sedimentary incinerator. Cont Shelf Res 26:2241–2259. https://doi.org/10.1016/j.csr.2006.07.016

Aller RC, Yingst JY (1978) Biogeochemistry of tube-dwellings – study of the sedentary polychaete *Amphitrite ornate* (Leidy). J Mar Res 36:201–254. https://elischolar.library.yale.edu/journal_of_marine_research/1429

Aller RC, Yingst JY, Ullman WJ (1983) Comparative biogeochemistry of water in intertidal *Onuphis* (Polychaeta) and *Upogebia* (Crustacea) burrows – temporal patterns and causes. J Mar Res 41:571–604. https://elischolar.library.yale.edu/journal_of_marine_research/1695

Aller RC, Heilbrun C, Panzeca C, Zhu ZB, Baltzer F (2004) Coupling between sedimentary dynamics, early diagenetic processes, and biogeochemical cycling in the Amazon-Guianas mobile mud belt: coastal French Guiana. Mar Geol 208:331–360. https://doi.org/10.1016/j.margeo.2004.04.027

Allison MA, Lee MT (2004) Sediment exchange between Amazon mudbanks and shore-fringing mangroves in French Guiana. Mar Geol 208:169–190. https://doi.org/10.1016/j.margeo.2004.04.026

Allison MA, Lee MT, Ogston AS, Aller RC (2000) Origin of Amazon mudbanks along the northeastern coast of South America. Mar Geol 163:241–256. https://doi.org/10.1016/s0025-3227(99)00120-6

Alongi DM (1997) Coastal ecosystem processes. CRC Press, Boca Raton. https://doi.org/10.1201/9781003057864

Anthony EJ, Gardel A, Gratiot N, Proisy C, Allison MA et al (2010) The Amazon-influenced muddy coast of South America: a review of mud-bank-shoreline interactions. Earth Sci Rev 103:99–121. https://doi.org/10.1016/j.earscirev.2010.09.008

Anthony EJ, Gardel A, Gratiot N (2014) Fluvial sediment supply, mud banks, cheniers and the morphodynamics of the coast of South America between the Amazon and Orinoco river mouths. Geol Soc London Spec Publ. https://doi.org/10.1144/SP388.8

Araújo JMC, Otero XL, Marques AGB, Nóbrega G, Silva JRF et al (2012) Selective geochemistry of iron in mangrove soils in a semi-arid tropical climate: effects of the burrowing activity of the crabs *Ucides cordatus* and *Uca maracoani*. Geo-Mar Lett 32:289–300. https://doi.org/10.1007/s00367-011-0268-5

Aschenbroich A, Michaud E, Stieglitz T, Fromard F, Gardel A et al (2016) Brachyuran crab community structure and associated sediment reworking activities in pioneer and young mangroves of French Guiana, South America. Estuar Coast Shelf Sci 182:60–71. https://doi.org/10.1016/j.ecss.2016.09.003

Aschenbroich A, Michaud E, Gilbert F, Fromard F, Alt A et al (2017) Bioturbation functional roles according to mangrove development in French Guiana, South America. Hydrobiologia 794:179–202. https://doi.org/10.1007/s10750-017-3093-7

Augustinus P (2004) The influence of the trade winds on the coastal development of the Guianas at various scale levels: a synthesis. Mar Geol 208:145–151. https://doi.org/10.1016/j.margeo.2004.04.007

Augustinus PGEF (1978) The changing shoreline of Surinam (South America). Publications of the Foundation for Scientific Research in Surinam and the Netherlands Antilles. Utrecht, The Netherlands

Baltzer F, Allison M, Fromard F (2004) Material exchange between the continental shelf and mangrove-fringed coasts with special reference to the Amazon-Guianas coast. Mar Geol 208:115–126. https://doi.org/10.1016/j.margeo.2004.04.024

Bertics VJ, Sohm JA, Treude T, Chow CET, Capone DG et al (2010) Burrowing deeper into benthic nitrogen cycling: the impact of bioturbation on nitrogen fixation coupled to sulfate reduction. Mar Ecol Prog Ser 409:1–15. https://doi.org/10.3354/meps08639

Brunier G, Michaud E, Fleury J, Anthony EJ, Morvan S et al (2020) Assessing the relationship between macro-faunal burrowing activity and mudflat geomorphology from UAV-based Structure-from-Motion photogrammetry. Remote Sens Environ 241:1–17. https://doi.org/10.1016/j.rse.2020.111717.111717

Doane TA, Horwath WR (2003) Spectrophotometric determination of nitrate with a single reagent. Anal Lett 36:2713–2722. https://doi.org/10.1081/al-120024647

Egawa R, Sharma S, Nadaoka K, MacKenzie RA (2021) Burrow dynamics of crabs in subtropical estuarine mangrove forest. Estuar Coast Shelf Sci 252:107244. https://doi.org/10.1016/j.ecss.2021.107244

Eisma D, Augustinus P, Alexander C (1991) Recent and sub recent changes in the dispersal of Amazon mud. Netherlands J Sea Res 28:181–192. https://doi.org/10.1016/0077-7579(91)90016-t

Forster S (1991) Die Bedeutung biogener Strukturen für den Sauerstoffffluß ins Sediment. Universität Kiel, Institute für Meereskunde

Froidefond JM, Pujos M, Andre X (1988) Migration of mud banks and changing coastline in French Guyana. Mar Geol 84:19–30. https://doi.org/10.1016/0025-3227(88)90122-3

Fromard F, Puig H, Mougin E, Marty G, Betoulle JL, et al. (1998) Structure, above-ground biomass and dynamics of mangrove ecosystems: new data from French Guiana. Oecologia 115:39–53. https://doi.org/10.1007/s004420050489

Gardel A, Proisy C, Lesourd S, Philippe S, Caillaud J et al (2009) A better understanding of mud cracking processes gained from in situ measurements on an intertidal mudflat in French Guiana. J Coast Res Special Issue 56:424–428. https://www.jstor.org/stable/25737611

Gensac E, Gardel A, Lesourd S, Brutier L (2015) Morphodynamic evolution of an intertidal mudflat under the influence of Amazon sediment supply - Kourou mud bank, French Guiana, South America. Estuar Coast Shelf Sci 158:53–62. https://doi.org/10.1016/j.ecss.2015.03.017

Gontharet S, Mathieu O, Leveque J, Milloux MJ, Lesourd S et al (2014) Distribution and sources of bulk organic matter (OM) on a tropical intertidal mud bank in French Guiana from elemental and isotopic proxies. Chem Geol 376:1–10. https://doi.org/10.1016/j.chemgeo.2014.03.009

Guimond JA, Seyfferth AL, Moffett KB, Michael HA (2020) A physical-biogeochemical mechanism for negative feedback between marsh crabs and carbon storage. Environ Res Lett 15:034024. https://doi.org/10.1088/1748-9326/ab60e2

Hall PO, Aller RC (1992) Rapid, small-volume, flow-injection analysis for ΣCO_2 and NH_4^+ in marine and fresh waters. Limnol Oceanogr 37:1113–1119. https://doi.org/10.4319/lo.1992.37.5.1113

Hamme RC, Emerson SR (2004) The solubility of neon, nitrogen and argon in distilled water and seawater. Deep-Sea Res I: Oceanogr Res Pap 51:1517–1528. https://doi.org/10.1016/j.dsr.2004.06.009

Iribarne O, Botto F, Martinetto P, Gutierrez JL (2000) The role of burrows of the SW Atlantic intertidal crab *Chasmagnathus granulata* in trapping debris. Mar Pollut Bull 40:1057–1062. https://doi.org/10.1016/s0025-326x(00)00058-8

Kana TM, Darkangelo C, Hunt MD, Oldham JB, Bennett GE et al (1994) Membrane inlet mass-spectrometer for rapid high-precision determination of N-2, O-2, and Ar in environmental water samples. Anal Chem 66:4166–4170. https://doi.org/10.1021/ac00095a009

Kristensen E (2008) Mangrove crabs as ecosystem engineers; with emphasis on sediment processes. J Sea Res 59:30–43. https://doi.org/10.1016/j.seares.2007.05.004

Kristensen E, Kostka J (2005) Macrofaunal burrows and irrigation in marine sediment: microbiological and biogeochemical interactions. Macro- and Microorganisms in Marine Sediments. Coast Estuar Stud 60:125–157. https://doi.org/10.1029/60CE08

Kristensen E, Mangion P, Tang M, Flindt MR, Holmer M et al (2011) Microbial carbon oxidation rates and pathways in sediments of two Tanzanian mangrove forests. Biogeochemistry 103:143–158. https://doi.org/10.1007/s10533-010-9453-2

Michaud E, Aschenbroich A, Gauthier O, Fromard F, Aller JY et al (2022) The codevelopment of mangroves and infaunal community diversity in response to the natural dynamics of mud deposition in French Guiana. Sustainability 14:2829. https://doi.org/10.3390/su14052829

Michaud E, Ashenbroich A, Stieglitz T, Brunier G, Aller RC, et al (2024) Small-scale spatial heterogeneity of crab burrows: an important parameter for accurate upscaling in mangrove ecosystem functioning. Regional Environmental Change (this issue)

Otero XL, Araújo JMC, Barcellos D, Queiroz HM, Romero DJ et al (2020) Crab bioturbation and seasonality control nitrous oxide emissions in semiarid mangrove forests (Ceará, Brazil). Appl Sci 10:1–16. https://doi.org/10.3390/app10072215

Proisy C, Gratiot N, Anthony EJ, Gardel A, Fromard F et al (2009) Mud bank colonization by opportunistic mangroves: a case study from French Guiana using LIDAR data. Cont Shelf Res 29:632–641. https://doi.org/10.1016/j.csr.2008.09.017

Ray R, Michaud E, Aller RC, Vantrepotte V, Gleixner G et al (2018) The sources and distribution of carbon (DOC, POC, DIC) in a mangrove dominated estuary (French Guiana, South America). Biogeochemistry 138:297–321. https://doi.org/10.1007/s10533-018-0447-9

Ray R, Thouzeau G, Walcker R, Vantrepotte V, Gleixner G, et al (2020) Mangrove-derived organic and inorganic carbon exchanges between the Sinnamary estuarine system (French Guiana, South America) and the Atlantic Ocean. J Geophys Res – Biogeosciences 125: 1-24 https://doi.org/10.1029/2020JG005739

Rine JM, Ginsburg RN (1985) Depositional facies of a mud shoreface in Suriname, South America - a mud analogue to sandy shallow-marine deposits. J Sediment Petrol 55:633–652. https://doi.org/10.1306/212F87A6-2B24-11D7-8648000102C1865D

Sarazin G, Michard G, Prevot F (1999) A rapid and accurate spectroscopic method for alkalinity measurements in seawater samples. Water Res 33:290–294. https://doi.org/10.1016/s0043-1354(98)00168-7

Smith NF, Wilcox C, Lessmann JM (2009) Fiddler crab burrowing affects growth and production of the white mangrove (*Laguncularia racemosa*) in a restored Florida coastal marsh. Mar Biol 156:2255–2266. https://doi.org/10.1007/s00227-009-1253-7

Soetaert K, Hofmann AF, Middelburg JJ, Meysman JR, Greenwood J (2007) The effect of biogeochemical processes on pH. Mar Chem 105:30–51. https://doi.org/10.1016/j.marchem.2006.12.012

Solórzano L (1969) Determination of ammonia in natural waters by phenolhypochlorite method. Limnol Oceanogr 14:799–801. https://doi.org/10.4319/lo.1969.14.5.0799

Stieglitz TC, Clark JF, Hancock GJ (2013) The mangrove pump: the tidal flushing of animal burrows in a tropical mangrove forest determined from radionuclide budgets. Geochim Cosmochim Acta 102:12–22. https://doi.org/10.1016/j.gca.2012.10.033

Strickland JDH, Parsons TR (1972) A practical handbook of seawater analysis. Fish Res Board Can Bull 167:1–310. https://doi.org/10.25607/OBP-1791

Waugh S, Aller RC (2017) N-2 production and fixation in deep-tier burrows of *Squilla empusa* in muddy sediments of Great Peconic Bay. J Sea Res 129:36–41. https://doi.org/10.1016/j.seares.2017.08.012

Waugh S, Aller RC (2021) Nitrogen cycling in muddy sediments of Great Peconic Bay, USA: seasonal N reaction balances and multi-year flux patterns. J Mar Res 79(4):149-179. https://elischolar.library.yale.edu/journal_of_marine_research/512

Wells JT, Coleman JM (1978) Longshore transport of mud by waves: northeastern coast of South America. Geol Mijnb 57:353–359

Xin P, Jin GQ, Li L, Barry DA (2009) Effects of crab burrows on pore water flows in salt marshes. Adv Water Resour 32:439–449. https://doi.org/10.1016/j.advwatres.2008.12.008

Ziebis W, Forster S, Huettel M, Jorgensen BB (1996) Complex burrows of the mud shrimp *Callianassa truncata* and their geochemical impact in the seabed. Nature 383:457–457. https://doi.org/10.1038/383457a0